

1 **Future projections of daily haze conducive and clear weather conditions over the North**
2 **China Plain using a Perturbed Parameter Ensemble**

3 Shipra Jain¹, Ruth M. Doherty¹, David Sexton², Steven Turnock^{2,3}, Chaofan Li⁴, Zixuan Jia¹,
4 Zongbo Shi⁵, Lin Pei⁶

5 ¹School of GeoSciences, The University of Edinburgh, Edinburgh, United Kingdom

6 ²Met Office Hadley Centre, Exeter, United Kingdom

7 ³University of Leeds Met Office Strategic (LUMOS) Research Group, School of Earth and
8 Environment, University of Leeds, UK

9 ⁴Center for Monsoon System Research, Institute of Atmospheric Physics, Chinese Academy of
10 Sciences, China

11 ⁵School of Geography, Earth and Environmental Sciences, University of Birmingham,
12 Birmingham, United Kingdom

13 ⁶Institute of Urban Meteorology, China Meteorological Administration, Beijing, China

14

15 **Corresponding Author:** Shipra Jain (Shipra.Jain@ed.ac.uk)

16 **Abstract**

17 We examine past and future changes in both winter haze and clear weather conditions over the
18 North China Plain (NCP) using a Perturbed Parameter Ensemble (PPE) and elucidate the
19 influence of model physical parameterizations on these future projections for the first time. We
20 use a large-scale meteorology-based Haze Weather Index (HWI) with values >1 as a proxy for
21 haze conducive weather and $\text{HWI} < -1$ for clear weather conditions over the NCP. The PPE
22 generated using the UK Met Office HadGEM-GC3 model shows that under a high-emission
23 (RCP8.5) scenario, the frequency of haze conducive weather ($\text{HWI} > 1$) is likely to increase
24 whereas the frequency of clear weather ($\text{HWI} < -1$) is likely to decrease in future. However, a
25 change of opposite sign with lower magnitude in the frequencies, though less likely, is also
26 possible. In future, the frequency of haze conducive weather for a given winter can be as much
27 as ~ 3.5 times higher than the frequency of clear weather over the NCP. The future frequencies
28 of haze conducive weather ($\text{HWI} > 1$) during winter are associated with changes in zonal-mean
29 mid-tropospheric winds and the vertical temperature gradient over the NCP. We also examined
30 the changes in the interannual variability of the haze conducive and clear weather, and find no
31 marked changes in the variability of future periods. We find a clear influence of model physical
32 parameterizations on climatological mean frequencies for both haze conducive and clear
33 weather. For mid to late 21st century (2033-2086), parametric effect can explain up to $\sim 80\%$
34 variance in climatological mean frequencies of PPE members. Therefore, model
35 parameterizations adds uncertainty in the future projections of haze conducive weather in
36 addition to the internal variability. We also find a growing influence of anthropogenic climate
37 change on future mean frequencies of haze conducive and clear weather over the 21st century
38 suggesting climate change can exacerbate the haze conducive weather and reduce the clear
39 weather conditions in future over the NCP.

40

41 **1. Introduction**

42 Over the last decade, a number of severe haze episodes (several days or longer) were
43 reported over the North China Plain (NCP) during boreal winter (December-January-February,
44 DJF). In January 2013, unprecedented PM_{2.5} levels exceeding 450 µg m⁻³ were observed over
45 the NCP (Wang et al., 2014a; Wang et al., 2014b; Zhang et al., 2018; Zhang et al., 2013).
46 Similar events were also observed in November-December 2015 when the PM_{2.5} concentrations
47 reached as high as 1000 µg m⁻³ in Beijing and caused the first-ever ‘red alert’ for severe air
48 pollution (Liu et al., 2017; Zhang et al., 2017). In December 2016, around 25% of the land area
49 of China was covered with severe haze for around one week (Yin and Wang, 2017). These
50 severe haze events adversely impacted public health including mortality, visibility, and
51 ultimately the economy of the country (Bai et al., 2007; Chen and Wang, 2015; Kan et al.,
52 2012; Kan et al., 2007; Wang et al., 2006; Xu et al., 2013; Hong et al., 2019).

53 Previous research has shown that the persistence of severe haze for days during winters
54 over the NCP occurred due to the combined effect of local and regional high pollutant
55 emissions and stagnant meteorological conditions (Li et al., 2018; He et al., 2016; Jia et al.,
56 2015; Pei et al., 2018; Zhang et al., 2021). The normal winter meteorological conditions over
57 the NCP are characterized by northwesterly flow near the surface through to the mid-
58 troposphere associated with the East Asian winter monsoon circulation (Fig. 1a and 1b; also
59 see An et al., 2019; Chen and Wang, 2015; Li et al., 2016; Renhe et al., 2014; Xu et al., 2006).
60 The northwesterly winds support the intrusion of relatively clean air from the high latitudes to
61 the NCP and therefore ventilate this region (Xu et al., 2006). However, during the severe haze
62 episodes, the near-surface northwesterlies appear to be weaker than normal and the mid-
63 tropospheric trough was reported to be shallower and shifted northwards – collectively leading
64 to a weaker than normal northwesterly flow and reduced horizontal transport of air pollutants
65 from the NCP (Fig. 2a-b). In addition to changes in horizontal winds, the vertical temperature

66 gradient between the lower and upper troposphere over the NCP can influence the vertical
67 dispersion of the pollutants. A warmer than normal temperature near the surface, accompanied
68 with colder temperature in the upper troposphere, would enhance the thermal stability and
69 reduce the atmospheric mixing leading to the build-up of the atmospheric pollutants over this
70 region (Fig. 2; also see Hou and Wu, 2016; Sun et al., 2014; Wang et al., 2014a; Zhang et al.,
71 2018; Cai et al., 2018). The planetary boundary layer height is also found to be suppressed
72 during extreme haze events leading to accumulation of pollutants, notably PM_{2.5} concentrations
73 (Liu et al., 2018; Petäjä et al., 2016), due to an increase in moisture, reduced vertical mixing
74 and dispersion which aids aerosol growth during high haze events over the NCP (An et al.,
75 2019; Tie et al., 2017).

76 On a daily scale, past studies have examined the changes in haze conducive weather
77 conditions over China under climate change scenarios using large-scale meteorology-based
78 indexes. For example, Cai et al. (2017) have used four key variables, i.e. meridional wind at
79 850 hPa (V_{850}), zonal wind at 500 hPa (U_{500}), temperatures at 850 hPa (T_{850}) and 250 hPa (T_{250})
80 pressure levels to calculate a meteorology-based daily Haze Weather Index (HWI). They have
81 projected a ~50% increase in the frequency of winter haze conducive weather conditions,
82 similar to the January 2013 event, over Beijing in the future (2050-2099) as compared to the
83 historical (1950-1999) period under the RCP8.5 scenario using 15 CMIP5 models. Using the
84 HWI, Liu et al. (2019) projected a 6-9% increase in the winter haze frequency under 1.5° and
85 2° global warming, respectively based on 20 CMIP5 models whereas Qiu et al. (2020)
86 projected a relatively high increase of 21% and 18% in severe winter haze episodes under 1.5°
87 and 2° global warming, respectively using an ensemble of climate simulations from the
88 Community Earth System Model 1 (CESM1) (Kay et al., 2015). Callahan and Mankin (2020)
89 also used specific humidity, V_{850} , T_{850} and temperatures at 1000 hPa to examine the haze
90 favourable meteorology for Beijing, and found a 10-15% increase in winter haze conducive

91 weather in CMIP5 multimodel and CESM large ensemble under 3° warming. These authors
92 have also emphasized a large influence of internal variability in addition to anthropogenic
93 forcing on future haze conducive weather over Beijing.

94 In addition to the large-scale meteorology based indexes, several other stagnation
95 indices based on regional or local meteorological variables have also been used to determine
96 the influence of anthropogenic climate change on haze conducive weather for China as well as
97 global regions. Using minimum monthly mean wind speeds averaged over northwestern
98 Europe, Vautard et al. (2018) suggested a potential increase in the frequency of stagnant
99 conditions conducive to air pollution over northwest Europe; however, their results were
100 sensitive to models used for the analysis. Horton et al. (2014) have used thresholds for the daily
101 mean near-surface (10-m) wind speeds, mid-tropospheric (500 hPa) temperatures and
102 accumulated precipitation to calculate the Air Stagnation Index (ASI) under RCP8.5 scenario
103 using 15 CMIP5 models. They found an increase in air stagnation occurrence events leading to
104 poor air quality by up to ~40 days per year over a majority of the tropics and sub-tropics. Han
105 et al. (2017) examined indicators of haze pollution potential (e.g. horizontal transport, wet-
106 deposition, ventilation conditions) using three regional climate simulations and projected a
107 higher probability of haze pollution risk over the Beijing-Tianjin-Hebei region under the
108 RCP4.5 scenario. Garrido-Perez et al. (2021) took a different approach as compared to
109 analysing probabilistic projections and used the ASI to generate stagnation storylines, i.e.
110 plausible and physically consistent scenarios of stagnation changes based on the response of
111 remote drivers under climate change forcing, for Europe and the United States (US).

112 While most studies indicate an increase in the haze conducive weather over China, a
113 few studies also find little impact of climate change on future projections of haze (Shen et al.,
114 2018; Pendergrass et al., 2019), which could partly arise due to the under-sampling of internal
115 variability associated uncertainty in their projections (Callahan and Mankin, 2020), as well as

116 model-to-model differences. Hence, there is a large uncertainty as to how haze conducive
117 weather conditions may change in the future and these depend on haze metrics or underlying
118 processes considered for future projections.

119 In order to account for the uncertainty in the future projections (e.g. of large-scale
120 circulation) particularly at the regional scale (Hawkins and Sutton, 2012; Deser et al., 2012;
121 Deser et al., 2014), it is desirable to use an ensemble of climate change simulations. Whilst a
122 multimodel ensemble, e.g. CMIP5 or CMIP6, is commonly used for climate change studies,
123 several other studies have also emphasised the use of an initialised ensemble or Perturbed
124 Parameter Ensemble (PPE) from a single model to assess the uncertainties and obtain a
125 comprehensive range of possible future climate realisations for the same emission scenario for
126 a given model (Knutti et al., 2010). All three methodologies have different advantages. For
127 instance, using multiple models allows us to sample structural uncertainty in future projections,
128 which cannot be sampled using a single model. On the other hand, using an initialised ensemble
129 from a single model allows us to sample a broader range of internal variability, which is often
130 under-sampled in a multimodel ensemble. The advantage of using the PPE over the initialised
131 or multimodel ensemble is that it not only accounts for internal variability but also model
132 uncertainty arising due to the different settings of the physical parameterisations in a single
133 model. Both multimodel ensemble and initialised ensemble from a single model have been
134 used to assess the future winter haze conducive conditions over Beijing. In this paper, we use
135 a PPE generated using the UK's Met Office HadGEM-GC3 model to assess for the first time
136 the impact of both model physical parameterisations and anthropogenic climate change on
137 future daily haze conducive weather conditions.

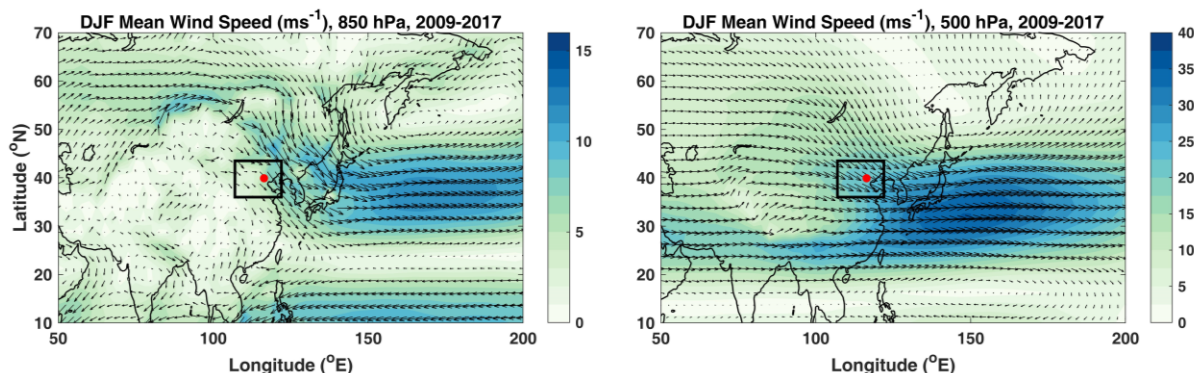
138 In this paper, our focus is on the daily haze conducive and clear weather conditions
139 over the NCP under a fixed high-emission scenario (RCP8.5). For this purpose, we use the
140 HWI proposed by Cai et al. (2018) as past research studies have shown a robust correlation

141 between the HWI, which is a large-scale meteorology based index, and haze conducive weather
142 for Beijing in China. Whilst Cai et al. (2018) originally proposed the HWI for Beijing, the
143 index is based on changes in large-scale meteorology over the NCP and thus offers a good
144 potential as the indicator of haze conducive weather over the NCP. One potential advantage of
145 using the HWI for future projections, as opposed to a regional or local air stagnation index, is
146 that the general circulation models generally simulate large-scale meteorology reasonably well
147 as compared to local or regional meteorology. Therefore, we expect the future projections of
148 clear or haze conducive weather provided using the HWI to be less uncertain than projections
149 provided using regional stagnation indexes.

150 The HWI uses four meteorological variables as stated above, but Cai et al. (2018) have
151 also examined the impact of the inclusion of more weather variables, such as geopotential
152 height, boundary layer thickness and local stratification instability, in the HWI and did not find
153 any significant differences in the performance of the HWI. Therefore, we use the same
154 variables and methodology as Cai et al (2018) to calculate the HWI and provide future
155 projections of haze conducive and clear weather using the HWI. However, our analysis is based
156 on an underlying assumption that the large-scale meteorological conditions, which are used as
157 a basis for the HWI, will have a similar influence on the air quality of the NCP in the future
158 climate as for present-day climate.

159 In this paper, we first examine the application of the HWI as a proxy for haze conducive
160 and clear weather over NCP for the current climate using a suite of observations (Section 3).
161 We then provide the projections of the haze conducive ($HWI > 1$) and clear weather ($HWI < 1$)
162 frequency over NCP for the historical and future period. We assess the impact of model
163 physical parametrisations and anthropogenic climate change on the frequencies (Section 4).
164 We also analyse the changes in the interannual variance of the frequency of haze conducive
165 and clear weather conditions for the future periods as compared to the historical period (Section

166 5). Finally, we assess the impact of parametric effect and anthropogenic climate change on
167 trends in haze conducive and clear weather occurrence over the 21st century (Section 6). Details
168 of data and methods used in this paper are provided in the next section.



169
170 **Figure 1** Average wind speed at (a) 850 hPa and (b) 500 hPa pressure level. The red dot
171 represents the location of Beijing and black rectangle shows the location of the NCP. This
172 figure has been repeated for a longer average period, i.e. 1979-2019 (not shown) and the result
173 is similar.

174 2. Data & Methods

175 2.1 Observations, Reanalysis Outputs and PPE Model Simulations

176 Hourly PM_{2.5} concentrations are used from the US embassy site for Beijing for DJF
177 from 2009-2017. Daily mean PM_{2.5} concentrations are constructed using hourly data to
178 evaluate the performance of the HWI as a representative of haze conducive and clear weather
179 conditions for Beijing (see Section 3). We also used newly released gridded daily PM_{2.5}
180 concentrations for DJF from Chinese Air Quality Reanalysis Datasets (CAQRA) provided by
181 China National Environment Monitoring Centre for 2013-2017 (Kong et al., 2021) to test the
182 performance of the HWI across entire China. The CAQRA data has been produced by
183 assimilating surface air quality observations from over 1000 monitoring sites in China and is
184 available at a high spatial resolution of around 15×15 km and hourly temporal resolution over
185 China. More details on the validation of the CAQRA dataset against the independent station
186 data is provided in Kong et al. (2021). The visibility data for Beijing (homogenized data for 20

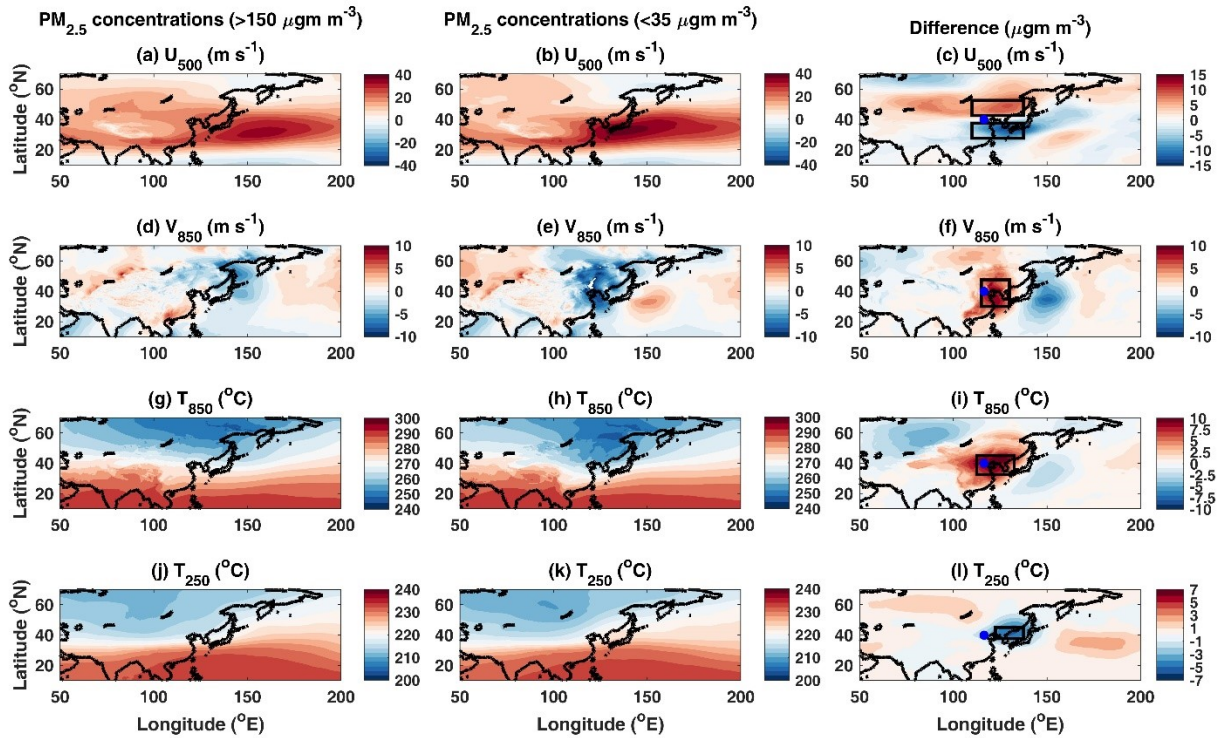
187 stations in Beijing) is provided by the National Meteorological Information Center of China,
188 China Meteorological Administration (CMA), for DJF 1999-2018.

189 We used daily ERA-5 reanalysis data of four variables: meridional wind at 850 hPa
190 pressure level (V_{850}), zonal wind at 500 hPa pressure level (U_{500}), temperatures at 850 hPa
191 level (T_{850}) and 250 hPa (T_{250}) to calculate the HWI for DJF 1979-2019. The ERA-5 data used
192 here is available at $0.25^\circ \times 0.25^\circ$ horizontal resolution and hourly temporal resolution
193 (Hersbach et al., 2020).

194 We used a PPE of climate simulations produced using the recent configuration of the
195 UK Met Office's HadGEM3-GC3.05 coupled model (Sexton et al., 2021; Yamazaki et al.,
196 2021). The base model used for PPE, HadGEM3-GC3.05, has a horizontal resolution of ~ 60
197 km with 85 vertical levels. A total of 47 model parameters from seven parameterization
198 schemes were simultaneously perturbed to obtain the PPE (the full list of perturbed parameters
199 is provided in Table 1 of (Sexton et al., 2021). Here, we used daily outputs of V_{850} , U_{500} , T_{850}
200 and T_{250} for DJF for the historical (1969-2005) and future (2006-2089) under the RCP8.5
201 scenario. In addition, we also assessed internal variability using 200-year control simulations
202 for each PPE member where 1900 boundary conditions were prescribed. Overall, 16 PPE
203 members are available for all the control, historical and RCP8.5 simulations

204 **2.2 Calculation of the HWI**

205 The winter HWI is calculated using the methodology given by Cai et al. (2017). We
206 analyse the composite differences in the U_{500} , V_{850} , T_{850} and T_{250} for hazy ($PM_{2.5}$ concentrations
207 $> 150 \mu\text{g m}^{-3}$ for Beijing) and clear ($PM_{2.5}$ concentrations $< 35 \mu\text{g m}^{-3}$ for Beijing) days across
208 China for DJF 2009-2017 (Fig. 2) (see section 3.1 for an explanation on the $PM_{2.5}$ concentration
209 cut-offs values used here). We also provide the composite values for these meteorological
210 variables for hazy and clear days separately in Fig. 2.



211

212 **Figure 2** Winter composites of u-wind at 500 hPa level (U_{500}) over China for all available days
 213 for which data is available from US embassy station for Beijing for DJF 2009-2017 for **(a)** high
 214 $PM_{2.5}$ ($>150 \mu\text{gm m}^{-3}$), **(b)** low $PM_{2.5}$ ($<35 \mu\text{gm m}^{-3}$) concentrations and **(c)** difference between
 215 the composites in (a) and (b). **(d-f)** same as (a-c) but for v-wind at 850 hPa level (V_{850}), **(g-i)**
 216 same as (a-c) but for temperature at 850 hPa level (T_{850}), and **(j-l)** same as (a-c) but for
 217 temperature at 250 hPa pressure level (T_{250}). Black rectangles (B1-B5) in the last column show
 218 the regions for which spatial means were used for the calculation of the HWI. The blue dot in
 219 these columns shows the location of Beijing.

220

During the hazy days, the mid-tropospheric westerly flow becomes weaker over the
 221 NCP as compared to the clear days (Fig. 2a-c). The mid-tropospheric trough also moves
 222 northwards as suggested by the dipole pattern in Fig 2c, which shows the differences in the
 223 U_{500} for hazy and clear days. The northerly flow near the surface is weaker during hazy days
 224 as compared to clear days (Fig. 2d-f). The lower troposphere is relatively warmer during hazy
 225 days as compared to clear days (Fig. 2g-i) whereas the upper troposphere is cooler over the
 226 NCP (Fig. 2j-l). The changes in these variables are also consistent with the previous studies
 227 (e.g. Cai et al., 2017) that showed similar changes for this time period. Therefore, we use these
 228 four variables for the calculation of the HWI, which is used as a proxy for haze conducive and
 229 clear weather conditions under a future climate.

230 For the calculation of observational HWI, we use ERA-5 reanalysis data for the period
231 1979-2019. We first create a daily DJF time series of each variable for each reanalyses grid
232 point over China. The daily DJF time series is concatenated for the period 1979-2019. A daily
233 standardised anomaly time series is created for each meteorological variable by first removing
234 the daily mean climatology from each day of the time series and then normalising by the
235 standard deviation. Spatial averages are then obtained over the relevant boxes (B1 to B5) for
236 each meteorological variable following Cai et al. (2017) (Fig. 1). The HWI time-series is
237 calculated by using the following equation:

$$238 \quad \text{HWI}(t) = U_{500}(t) + V_{850}(t) + dT(t)$$

239 where $U_{500} = U_{500,B1}(t) - U_{500,B2}(t)$, $V_{850} = V_{850,B3}(t)$, and $dT = T_{850,B4}(t) - T_{250,B5}(t)$. The HWI
240 (t) time series is then itself normalized by its own standard deviation.

241 For the PPE historical and RCP8.5 simulations, the daily HWI time series is calculated
242 for each ensemble member for DJF for 1969-2089 using the same methodology as used for
243 ERA-5, with the difference being that the normalisation of the PPE time-series (1969-2089) is
244 performed using the historical standard deviation (1969-2005), following Cai et al. (2017).
245 Similarly, the HWI time series is calculated for the PPE pre-industrial control simulations for
246 170 model years out of 200 model years (the first 30 years are discarded as model spin-up
247 period). The normalisation of the pre-industrial control time series is performed using the
248 standard deviation for 170 years. The pre-industrial control simulations used here are initialised
249 with past forcings corresponding to the year 1900 and therefore are an approximate
250 representation of the internal variability of the current climate as this does not take into account
251 any temporal changes in the internal variability from 1900 to the historical and future periods
252 used here.

253 **3. Haze Weather Index as an indicator for clear and haze conducive weather conditions**
254 **over the NCP**

255 As the HWI was originally proposed for Beijing by Cai et al. (2018), we first determine
256 if the HWI can be used as a representative of haze conducive and clear weather conditions for
257 the present climate for Beijing using (a) PM_{2.5} concentrations from the US embassy station in
258 Beijing and (b) PM_{2.5} concentrations averaged over larger Beijing domain from CAQRA
259 reanalysis and (c) visibility data from the CMA stations in Beijing. We then determine the
260 spatial extent of the region for which HWI can be used as an indicator of haze conducive and
261 clear weather conditions using PM_{2.5} concentrations for China using CAQRA reanalysis data.
262 We use the 25th and 75th percentile values of daily mean PM_{2.5} concentrations to identify the
263 clear and hazy days, respectively for each dataset. For visibility, we use the opposite criterion,
264 i.e. 25th percentile as a threshold for hazy days and 75th percentile as a threshold of clear days,
265 as lower visibility is associated with hazy days and higher visibility with clear days. The days
266 with daily PM_{2.5} concentration or visibility lying between the 25th and 75th percentile values
267 are identified as moderately polluted days.

268 **3.1 PM_{2.5} concentrations for Beijing versus HWI**

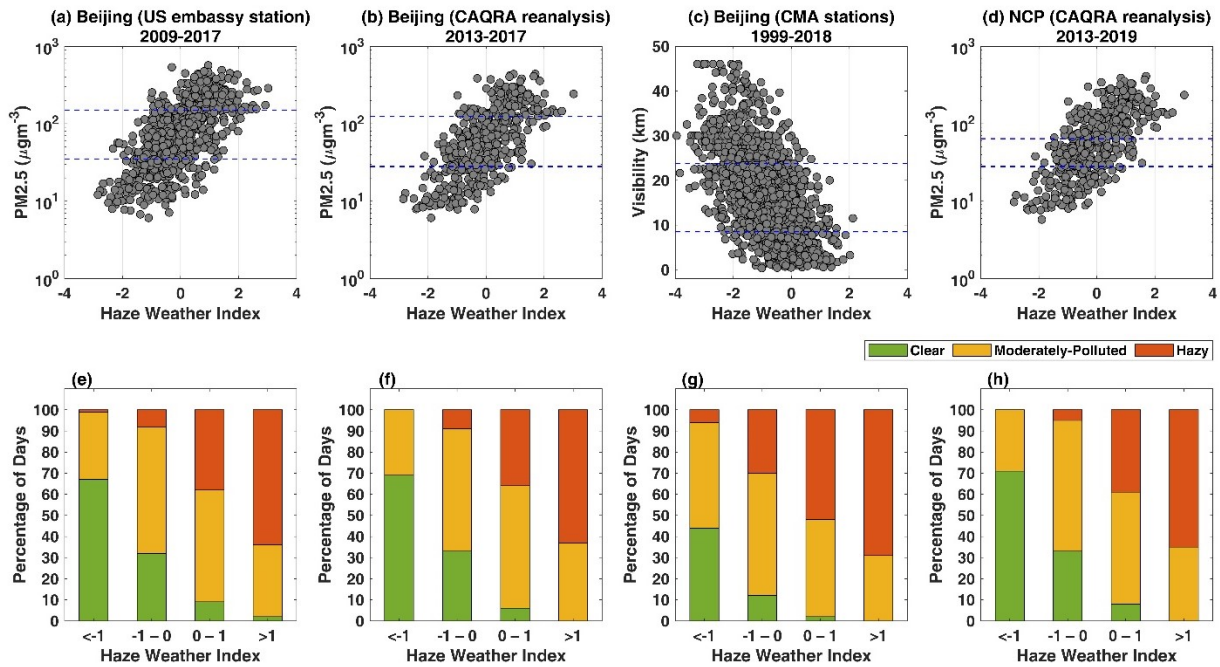
269 We examine the relationship between the daily HWI and PM_{2.5} concentrations for the
270 US embassy station for Beijing. Figure 3 (a) shows that the daily HWI increases linearly with
271 increasing PM_{2.5} concentrations for up to ~150 µg m⁻³ and PM_{2.5} > 150 µg m⁻³, the HWI starts
272 to level-off (note the log scaling in the y-axis). The time-series correlation between the HWI
273 and PM_{2.5} concentration is ~0.58, which is significant at the 1% level. Callahan et al. (2019)
274 have also obtained a correlation coefficient of 0.58 for daily PM_{2.5} concentrations from the U.S.
275 embassy in Beijing and the HWI calculated using NCAR R1 reanalysis.

276 The 25th and 75th percentile values of daily mean PM_{2.5} concentrations for the US
277 embassy Beijing station for DJF 2009-2017 are ~35 and ~150 $\mu\text{g m}^{-3}$ respectively. We
278 determine the percentage of hazy days (with daily mean PM_{2.5} concentrations $>150 \mu\text{g m}^{-3}$) and
279 clear days (with daily mean PM_{2.5} concentrations $< 35 \mu\text{g m}^{-3}$) for different HWI ranges (Fig.
280 3e). Out of all days with HWI >1 , 64% have daily mean PM_{2.5} concentrations $> 150 \mu\text{g m}^{-3}$ and
281 98% with PM_{2.5} concentrations $>35 \mu\text{g m}^{-3}$. This suggests that for HWI >1 , almost all days are
282 hazy or moderately polluted. Similarly, almost all days with HWI < -1 are clear or moderately
283 polluted. Using HWI thresholds of ± 1 demarcates between the clear and hazy days, i.e. almost
284 no clear days occur for HWI >1 and almost no hazy days occur for HWI <-1 .

285 We have also examined the relationship between the individual variables in the HWI
286 (section 2.2) and PM_{2.5} concentrations observed at the US embassy in Beijing/CAQRA and
287 find that the individual components have correlation values that are similar to or less than that
288 of those used in the combined HWI. Also, physically multiple favourable weather conditions,
289 as represented by each of these variables, collectively provide a conducive setting for haze.
290 Hence, we focus on the HWI as a combined index rather than its individual components.

291 To examine if the PM_{2.5} concentrations from the US embassy station are sensitive to
292 the abrupt changes in the local meteorology, e.g. wind speeds or direction, we also examine
293 the relationship between the HWI and PM_{2.5} concentrations averaged over the domain centred
294 around Beijing (116.15 – 116.65 °E, 39.65 – 40.15 °N) from the CAQRA reanalysis data (Fig.
295 3b and 3f). The PM_{2.5} concentrations for region spatially averaged around Beijing from
296 CAQRA data are in the range $6 \mu\text{g m}^{-3} - 441 \mu\text{g m}^{-3}$ and from the Beijing US embassy station
297 are $6 \mu\text{g m}^{-3} - 569 \mu\text{g m}^{-3}$ suggesting the values from both data sources are comparable. The
298 correlation coefficient is ~0.58, which is the same as the correlation obtained using the US
299 embassy data. The total number of hazy, clear and moderately polluted days for different HWI

300 ranges also show similar results for both datasets (Fig. 3e-3f). This implies that the HWI
 301 relationship with PM_{2.5} concentrations is robust across different data sources and that PM_{2.5} is
 302 a regional pollutant.



303 **Figure 3** HWI versus daily mean (a) PM_{2.5} concentrations for the US embassy Beijing station for DJF
 304 2009-2017 (b) PM_{2.5} concentrations spatially averaged over the region around Beijing (116.15-116.65
 305 °E, 39.65 - 40.15 °N) from CAQRA reanalysis for DJF 2013-2017 (c) visibility averaged over 20
 306 stations from the CMA for DJF 1999-2018 and (d) PM_{2.5} concentrations spatially averaged over the
 307 NCP (36-43.5 °N, 107-122 °E) from CAQRA reanalysis. Blue lines show the 25th and 75th percentile
 308 thresholds used to define clear and hazy days for each dataset. Percentage of clear, moderately polluted
 309 and hazy days for different HWI ranges for the (e) US embassy Beijing station for DJF 1999-2018 (f)
 310 larger Beijing domain (116.15-116.65 °E, 39.65 - 40.15 °N) from CAQRA reanalysis for DJF 2013-
 311 2017 (g) Beijing for DJF 1999-2018 (h) NCP from the CAQRA reanalysis for DJF 2013-2017.

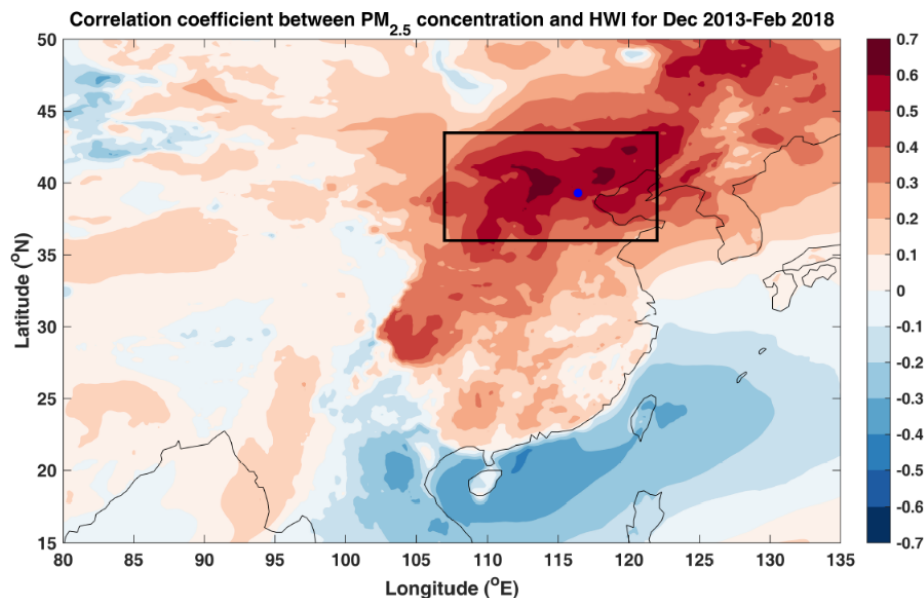
313 3.2 Visibility for Beijing versus HWI

314 As visibility is an optical representative of haze (Wang et al., 2006) and the data for
 315 visibility is available for a relatively long period (1999-2018) as compared to the PM_{2.5}
 316 concentrations, we also correlate the HWI with the visibility over Beijing. Figure 3 (c) shows
 317 that the HWI is inversely related to the visibility for the Beijing station. The time-series
 318 correlation between the HWI and visibility is -0.63, which is significant at the 1% level. The
 319 days with visibility < 8.5 km are identified as hazy days, days with visibility > 23.8 km are
 320 identified as clear days. For days with HWI > 1, no clear days occur and similarly for days with

321 HWI < -1, only 6% of days are hazy (Fig 3g). This further confirms that the correlation between
322 the HWI and haze is significant for a longer period (1999-2018) using visibility as a metric for
323 haze (alternative to the PM_{2.5} concentrations used above).

324 3.3 PM_{2.5} concentrations over North China Plain versus HWI

325 We now determine the spatial extent for which HWI can be used as an indicator of haze
326 clear or haze conducive conditions using PM_{2.5} concentrations from CAQRA reanalysis. We
327 correlate the daily time-series of PM_{2.5} concentration at each grid point with the HWI for DJF
328 2013-2017 (Fig. 4). Over the entire NCP (36-43.5 °N, 107-122 °E), the correlation coefficient
329 between the daily HWI and gridded PM_{2.5} concentration is ~0.7, significant at the 1% level.
330 The correlation is considerably lower but still significant over other eastern China regions, e.g.
331 north easternmost China and the Sichuan Basin (27-32 °N, 102-107 °E).



332
333 **Figure 4** Spatial distribution of correlation between winter PM_{2.5} concentrations and HWI time series
334 at each grid point. Blue dot shows the Beijing station (39.3 °N, 116.4 °E) and the black rectangle shows
335 the North China Plain (36-43.5 °N, 107-122 °E).

336 Considering daily mean PM_{2.5} concentrations averaged over the NCP, we also find a
337 linear relationship with the daily HWI ($r = 0.66$; significant at the 1% level; Fig 2d). We also
338 calculate the percentage of clear and hazy days for different HWI ranges for the larger domain

339 of the NCP using the 25th and 75th percentile values, respectively. The percentage of hazy and
340 clear days for $\text{HWI} > 1$ and $\text{HWI} < -1$ for NCP in CAQRA reanalyses are very similar to the
341 values obtained for the US embassy Beijing station (Fig 3h).

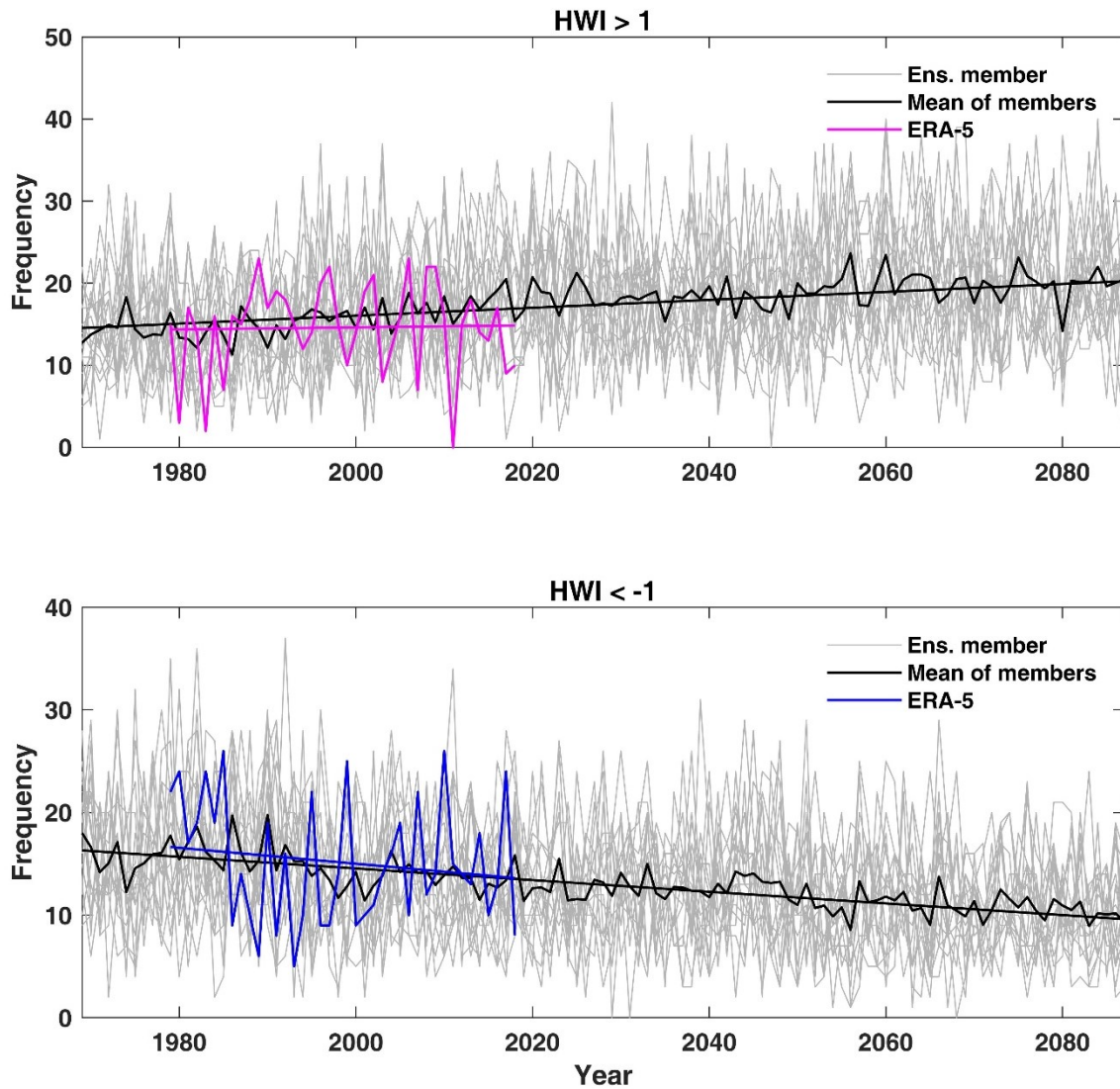
342 Overall, our results confirm that the daily HWI has a robust relationship with daily
343 $\text{PM}_{2.5}$ concentrations not only for the Beijing station but across the NCP for the given time
344 periods. Therefore, we use $\text{HWI} > 1$ as a proxy for haze conducive weather and $\text{HWI} < -1$ as a
345 proxy for clear weather across the NCP region. This threshold is also consistent with several
346 other studies (e.g., Cai et al., 2017; Callahan and Mankin, 2020; Callahan et al., 2019), that
347 have used $\text{HWI} > 1$, as a cut-off for haze conducive weather for Beijing. We now calculate the
348 frequency of haze conducive weather ($\text{HWI} > 1$) and clear weather ($\text{HWI} < -1$) for the past and
349 future using ERA-5 reanalysis and PPE members.

350 **4. Historical and future changes in haze conducive and clear weather occurrence**

351 The frequency of haze conducive weather ($\text{HWI} > 1$) and clear weather ($\text{HWI} < -1$) from
352 the ERA-5 reanalyses and the PPE are shown in Fig. 5. For ERA-5, the frequency of haze
353 conducive weather has increased, whereas the frequency of clear weather ($\text{HWI} < -1$) has
354 reduced for the period 1979-2018. The mean frequency of haze conducive weather using 16
355 PPE members shows a relatively larger increase than ERA-5 for the same 1979-2018 time
356 period (Fig. 5a). In contrast, the mean frequency of clear weather from the PPE for this period
357 shows a similar reduction to that obtained using the ERA-5 reanalyses (Fig. 5b).

358 We examine the changes in the frequency of haze conducive weather ($\text{HWI} > 1$) and
359 clear weather ($\text{HWI} < -1$) for the historical (1979-2005) and three future periods, i.e. near (2006-
360 2032), mid (2033-2059) and far (2060-2086) future. The mean frequency for haze conducive
361 weather is 14.7 days per winter obtained from the ERA-5 reanalysis and 15.0 days per winter
362 from the PPE mean for the historical period. The corresponding values for clear weather are

363 15.0 days and 15.2 days per winter for ERA-5 and PPE, respectively. This shows a good
 364 agreement between the mean frequencies of haze conducive and clear for the ERA-5 data and
 365 the PPE mean for the historical period.

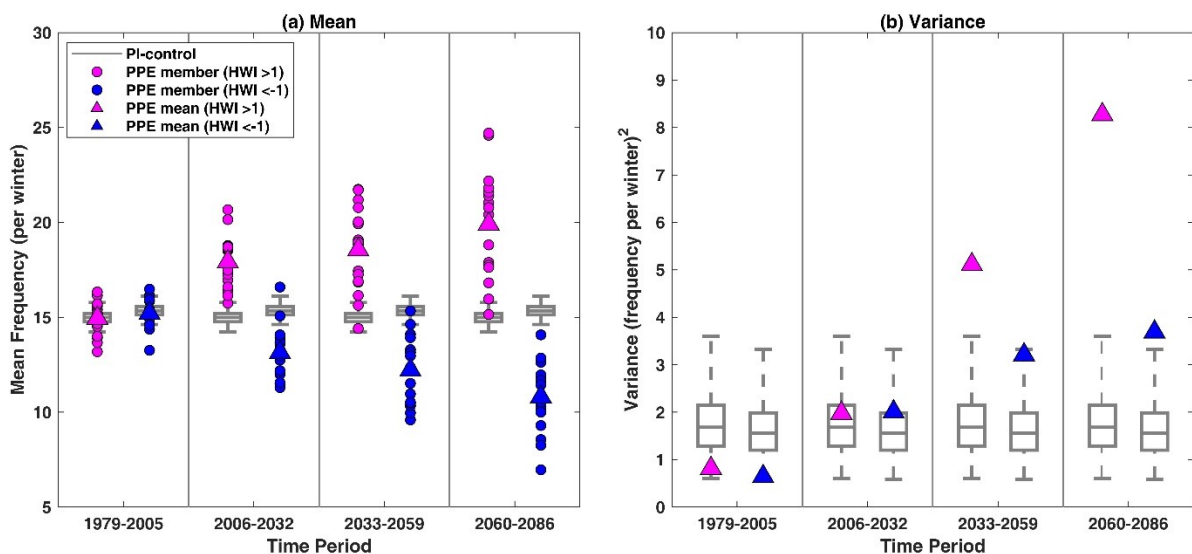


366

367 **Figure 5** Frequency of haze conducive weather (HWI>1, pink line) and clear weather (HWI<-1, blue
 368 line) per winter from ERA-5 reanalysis (1979 to 2018). Year 1979 represents period from 1 December
 369 1979 to 28 February 1980 and so on. For each winter (DJF), we calculate the total number of days with
 370 HWI>1 as proxy for haze conducive weather and HWI < -1 as proxy for clear weather conditions. Grey
 371 lines show frequencies from 16 individual PPE members and black line shows the mean of frequency
 372 using all 16 PPE members for 1969-2087 under the RCP8.5 scenario. Linear trend is calculated using
 373 the line of best fit.

374 The mean frequency of haze conducive weather for near, mid and far future is 17.9,
 375 18.6 and 19.9, respectively. The mean frequency for the same future periods for clear weather

376 is 13.2, 12.2 and 10.8, respectively (Fig. 6a). The mean change in the frequency of haze
 377 conducive weather averaged across all PPE members is 20%, 24% and 33% for the near, mid
 378 and far future respectively as compared to the historical period, suggesting that the frequency
 379 of haze conducive weather will likely increase for all future periods (Fig. 6a). However, there
 380 exists a very large range in the projected change for all three future periods suggesting internal
 381 variability or parametric effect could influence the future projections of haze conducive
 382 weather. For the near and mid future, days with $HWI > 1$ are projected to change by -1% to 41%
 383 and -12% to 65% across the 16 PPE members, respectively, as compared to the frequency for
 384 the historical period. For the far future, the range of projected change is even larger, and an
 385 increase of $\sim 87\%$ in the frequency of haze conducive weather is also possible. It is noted that,
 386 for all three periods, only one of the sixteen ensemble members (E16 shown in Fig. 10) shows
 387 a reduction in the haze conducive weather frequency whereas other ensemble members show
 388 an increase in frequency for all periods. For the historical period, E16 ensemble member has a
 389 mean frequency of 16.3, which reduces to 16.2, 14.4 and 15.2 for near, mid and far future.
 390 While E16 ensemble member shows a consistent reduction in mean frequency in future, the
 391 reduction is specific to only this ensemble member and is not a general feature across PPE
 392 members.



393

394 **Figure 6 (a)** Mean frequency of haze conducive weather ($HWI > 1$, pink) and clear weather ($HWI < -1$,
395 blue) for the historical period (1979-2005), near (2006-2032), mid (2033-2059) and far (2060-2086)
396 future under the RCP8.5 scenario. Circles represent PPE members and triangles PPE mean. Grey box
397 and whiskers show the distribution of 10,000 values of mean frequencies sub-sampled from the control
398 simulation, **(b)** same as (a) but shows variance across 16 PPE members for each period. For box and
399 whiskers, we first randomly sampled 10,000 time series of length 27 years using 2704 years of pre-
400 industrial control simulation and calculated 10,000 values of mean frequency. We then randomly sub-
401 sample 16 mean values (corresponding to the number of ensemble members) from the 10,000 mean
402 values, calculated their mean for (a) and variance for (b). This is repeated 10,000 to obtain a distribution.
403 The boxes are at the 25th and 75th percentile and the whiskers at 2.5th and 97.5th percentile of mean and
404 variance distribution. For panel (a), the box and whiskers are comparable only to the ensemble means
405 (triangles) and not ensemble members (circles).

406 For clear weather ($HWI < -1$), the mean change in the frequency averaging across all
407 PPE members is -13%, -20% and -29% for near, mid and far future, respectively (Fig 6a).
408 Considering the range across the 16 PPE members, the frequency of clear weather for near,
409 mid and far future is projected to change by -29% to 25%, -36% to 10% and -57% to -9%,
410 respectively. Overall, most ensemble members show an increase in the frequency of haze
411 conducive weather and a reduction in the frequency of clear weather for all three future periods.
412 However, negligible change or even the opposite change, though less likely, but possible for
413 all periods.

414 We also determine the influence of anthropogenic climate change and the parametric
415 effect on the frequencies of haze conducive weather ($HWI > 1$) and clear weather ($HWI < -1$) for
416 the historical as well as the three future periods. As shown in later Section 5, the estimate of
417 interannual variance from the control is representative of all time periods and shows no
418 discernible parametric effect. Therefore, we pool the 16 PPE control simulations to sample the
419 internal variability for box and whiskers shown in Fig. 6 (a) and 6 (b) (see captions for details
420 on resampling).

421 In Fig. 6 (a), we show the mean frequency of haze conducive weather and clear weather
422 for 16 individual PPE members (circles) and PPE mean (triangles). The grey box and whiskers
423 represent the range of ensemble mean frequencies that can be explained by the internal

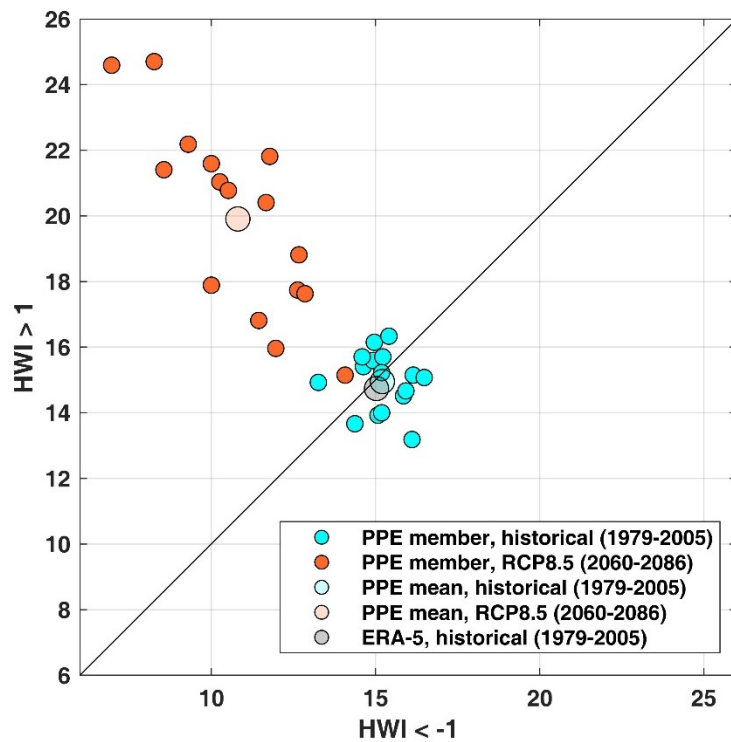
424 variability. If the PPE mean (triangles) lies within the whiskers (i.e. 95 percentile of the control
425 distribution) we conclude no influence of anthropogenic climate change on mean frequency
426 however if the PPE mean lies outside the whiskers, it would represent a climate change signal
427 in the mean frequency. Figure 6 (a) suggest that the mean frequencies for haze conducive as
428 well as clear weather lies within the box-whiskers for the historical but lies outside the whiskers
429 for the three future periods, thereby showing a clear impact of anthropogenic climate change
430 on the frequencies of both haze conducive and clear weather conditions.

431 We now examine whether the differences in the mean frequency across different PPE
432 members (shown by circles in Fig. 6a) for a given period can be explained by the internal
433 variability or if the differences in PPE members partly arise due to the parametric effect. The
434 triangles in Fig. 6b shows the variance across 16 PPE members, i.e. variance across 16 circles
435 shown in Fig. 6a, for each time period. The whiskers in Fig. 6b show the 95th confidence
436 interval from the control simulation and is representative of the internal variability. For any
437 time period, if the PPE member variance (triangle) lies within the whiskers, we conclude that
438 the differences in mean frequencies in Fig. 6a can be fully explained by the internal variability
439 and there is no discernible impact of the parametric effect. However, if the triangles lie outside
440 the whiskers in Fig. 6b, we conclude an impact of the parametric effect on the mean frequency
441 for that period. For the points that lie outside the whiskers in Fig. 6b, we also quantify the
442 percentage of variance that can be explained by the internal variability and parametric effect.
443 For any time period, the variance in ensemble mean due to the parametric effect is simply
444 calculated as follow and the remaining variance is attributed to the internal variability.

$$445 \quad \frac{\text{Total variance in the ensemble mean} - \text{Mean variance from the control simulation}}{\text{Total variance in the ensemble mean}} \times 100$$

446 Figure 6b shows that the variance in PPE mean frequency for historical and future
447 periods lies within the range sampled by the internal variability for both haze conducive

448 weather ($HWI > 1$) and clear weather ($HWI < -1$). For mid-future, the variance in haze conducive
 449 weather lies outside the whiskers and whereas the variance for clear weather lies within the
 450 whiskers. For mid-future and for haze conducive weather, the internal variability can explain
 451 $\sim 33\%$ of the variance across PPE members and the remaining $\sim 67\%$ arises due to the parametric
 452 effect. For the far future, triangles corresponding to both haze conducive and clear weather lies
 453 well outside the whiskers and therefore show a clear influence of parametric effect. Only $\sim 20\%$
 454 of the variance in the frequency of haze conducive weather and $\sim 43\%$ variance in the frequency
 455 of clear weather can be explained by the internal variability and the remaining 80% and 57%
 456 respective variance in the frequencies arise due to the parametric effect.



457

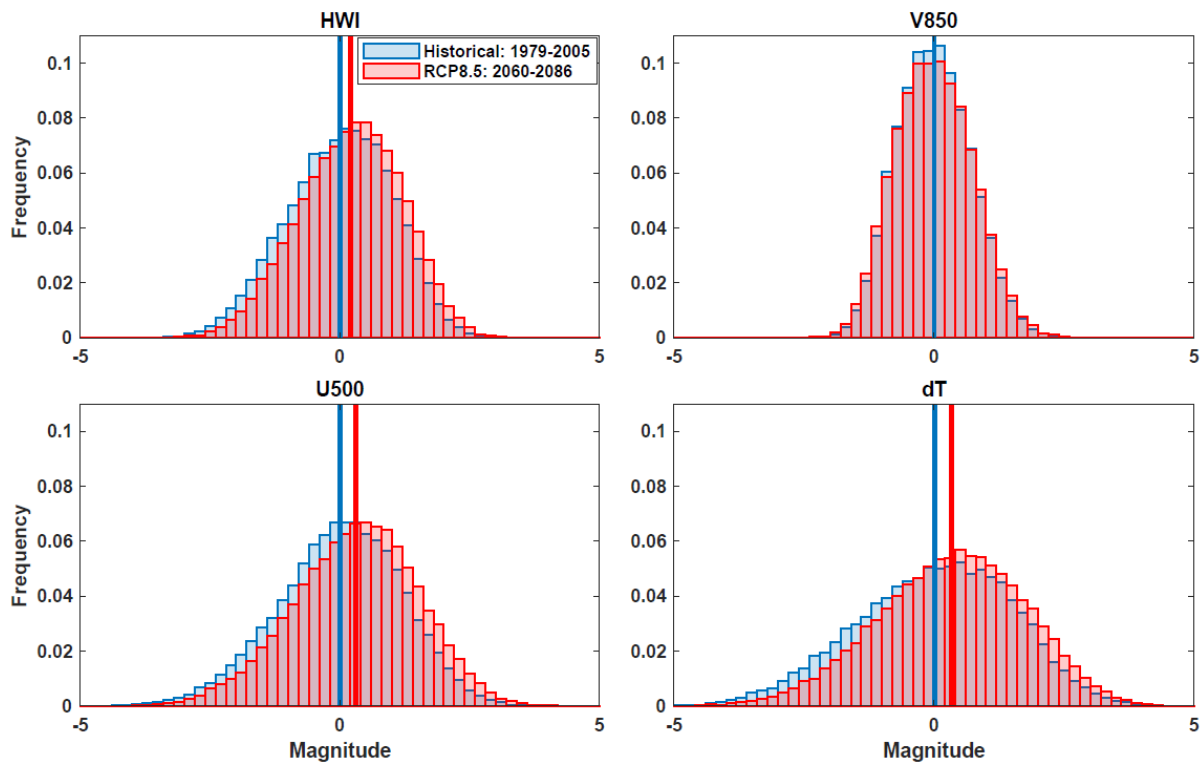
458 **Figure 7** Frequency of haze conducive weather ($HWI > 1$) versus clear weather ($HWI < -1$) averaged over
 459 the historical period (1979-2005) and the far-future (2060-2086) period under RCP8.5 using all PPE
 460 members. Circles denote individual PPE members whereas triangles denote the mean of the members.
 461 Grey triangle shows mean frequency from ERA-5 reanalysis for the historical period (1979-2005). The
 462 black solid line shows the 1:1 (identity) line.

463 In addition to the changes in the frequencies over time, we also investigate the relative
 464 changes in the frequency of haze conducive weather ($HWI > 1$) versus clear weather ($HWI < -1$).

465 The average haze conducive and clear weather frequency over the historical period are almost
466 equal for each PPE member (Fig. 7). All PPE members show a higher frequency for haze
467 conducive weather than clear weather under the far future (2060-2085), however, there exists
468 a substantial range in this change. The frequency of winter haze conducive weather can be
469 similar or up to 3.5 times the frequency of clear weather conditions (Fig. 7). Similar results are
470 also obtained for the near and mid-future. Averaged across the PPE members, the number of
471 haze conducive days can increase by ~ 2 times as compared to the number of clear days in
472 future. As noted in Fig. 7, the spread in the haze conducive weather frequency amongst
473 individual ensemble members is also larger for the far future (2060-2086) compared to the
474 historical period. This suggests a larger uncertainty and a larger range of possible future
475 meteorological conditions affecting haze and air quality as compared to the historical period.
476 Other studies have (e.g., Cai et al., 2017; Callahan and Mankin, 2020) also found similar
477 increases in the frequency of haze conducive weather for the future. However, the range of
478 projected change differs substantially across models as well as ensemble members. In our
479 study, in addition to the frequency of haze conducive weather, we also evaluate the changes in
480 the frequency of clear weather across different future periods and compared the relative
481 changes in both the frequencies, which is not examined in the past studies.

482 We now investigate changes in the distribution of the HWI as well as individual
483 constituents of the HWI between the far future (2060-86) and the historical (1979-2005) period.
484 The probability distribution of the HWI shows a shift in the distribution towards higher
485 magnitudes for the far future as compared to the historical period (Fig. 8). This implies an
486 increased frequency of haze conducive weather, as the number of days with $\text{HWI} > 1$ increase.
487 A similar shift is apparent in the zonal-mean wind (U_{500}) and the vertical temperature profiles
488 (dT), whereas no apparent shift is noted in V_{850} . We also find that the shift in the HWI, as well
489 as U_{500} and dT distribution, is not due to the shift in one particular PPE member or time period.

490 It is consistent across the 16 PPE members and is continual over time from the historical to the
 491 far-future period. Therefore, for the PPE analysed here, the changes in the haze conducive
 492 weather ($HWI > 1$) is largely associated with the changes in the U_{500} and dT , and V_{850} appear to
 493 have a less important role. Despite using a multimodel ensemble and a different time period
 494 than used here, a similar result with a relatively larger shift in the PDFs of U_{500} and dT as
 495 compared to V_{850} can also be noted in the Cai et al. (2017).



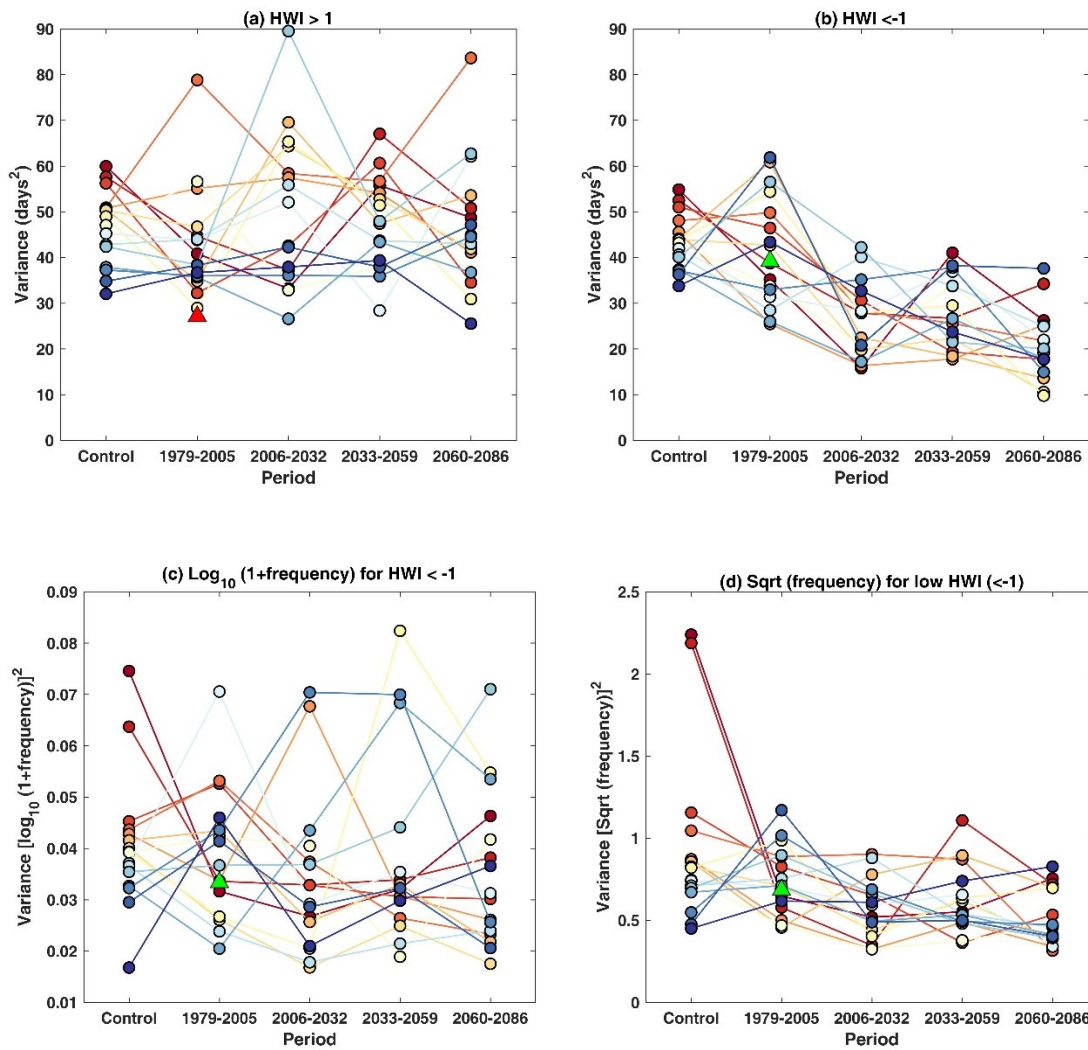
496

497 **Figure 8** Probability Distribution Functions (PDF) for the winter HWI, meridional winds at
 498 850 hPa pressure level (V_{850}), zonal winds at 500 hPa pressure level (U_{500}) and temperature
 499 gradient between the lower and upper troposphere (dT). The PDF for the HWI is created using
 500 the daily DJF time series of all 16 PPE members. PDFs for V_{850} , U_{500} and dT are created using
 501 the normalized daily DJF time series of each variable calculated for the HWI (see section 2.2
 502 for details) and represents the constituent variables of the HWI. Blue bars show the PDFs for
 503 the historical period and red for the far future under the RCP 8.5 scenario. Blue and red solid
 504 lines show the mean values of the PDF for historical and far future, respectively.

505 **5. Interannual variability in haze conducive and clear weather frequency**

506 Large interannual variability in the frequency of haze conducive ($HWI > 1$) and clear
 507 weather ($HWI < -1$) is apparent in both individual PPE members and ERA-5 reanalysis (Section

508 4). Therefore, we examine the changes in the interannual variance of the frequencies for future
 509 periods as compared to the historical period. We also compare the variance in historical and
 510 future time periods with the variance in the control simulation to discern the influence of the
 511 model physical parameterisations, i.e. parametric effect, on the variance.



512

513

514 **Figure 9** Interannual variance in frequency of winter (a) haze conducive weather (HWI>1) and (b)
 515 clear weather (HWI<-1) for the control simulation, historical (1979-2005), and near (2006-2032), mid
 516 (2033-2059) and far-future (2060-2086) under RCP8.5 for all 16 PPE members. Coloured circles are
 517 for individual PPE members and triangles for ERA-5 reanalysis. (c-d) are same as (b) but with \log_{10}
 518 and square root power transformations. For (c-d), we first calculate the \log_{10} of (1+frequency) and
 519 square-root of the frequency of clear days for the control simulation and each time-period, and then
 520 estimate variance for each respective period. The length of control simulation and all future periods is
 521 the same as historical, i.e. 27 years. The 27 years used for control here are randomly selected from 170-
 522 year control simulation for each member.

523 The interannual variance for ERA-5 data is 27 days² and 39 days² for haze conducive
524 and clear weather, respectively, for the historical period (1979-2005) (triangles in Fig. 9a-b).
525 The interannual variance in haze conducive weather frequency derived from the PPE members
526 for the historical period is larger than that for the ERA-5, whereas for the clear weather the
527 variance for ERA-5 lies within the range of the PPE members. No consistent change in the
528 interannual variance of haze conducive weather is noted for any of the PPE members (note the
529 changes in colour ranking) from the historical to the future periods suggesting little influence
530 of the parametric effect on the interannual variance of haze conducive weather.

531 In contrast, the frequency of clear weather for most PPE members show a marked
532 reduction in the interannual variance from historical to near-future (Fig. 9b). However, as the
533 frequency of clear weather show a decreasing trend in time (see Fig. 5b), the mean frequency
534 would be expected to reduce for the three future periods. Also, the reduction in variance could
535 arise as the frequencies of clear weather approach their lower bound of zero. With count data,
536 a power transformation is often applied to stabilize the variance across all time periods. We
537 applied two power transformations, i.e. $\log_{10}(1+x)$ and square-root (x), where x is the count
538 data (Fig. 9c-d). We find the spread in the variance in the control simulation across the PPE
539 members is comparable with the historical as well as future periods (Fig. 9c-d). Note that for
540 control simulation we randomly selected 27 years (length same as historical and future periods)
541 from 170 years of control simulation from each PPE member, however, we note comparable
542 variance for the other randomly selected samples. Figure 9 (c-d) also shows that the individual
543 PPE members show inconsistent changes in the variance (noting changes in the colour ranking)
544 from control to historical and future periods. Therefore, no robust changes in the interannual
545 variance of haze conducive and clear weather can be detected from control to historical and
546 future periods. This means we can use the variance in the control simulation as a representative
547 estimate of internal variability. This enables us to quantify the influence of the parametric effect

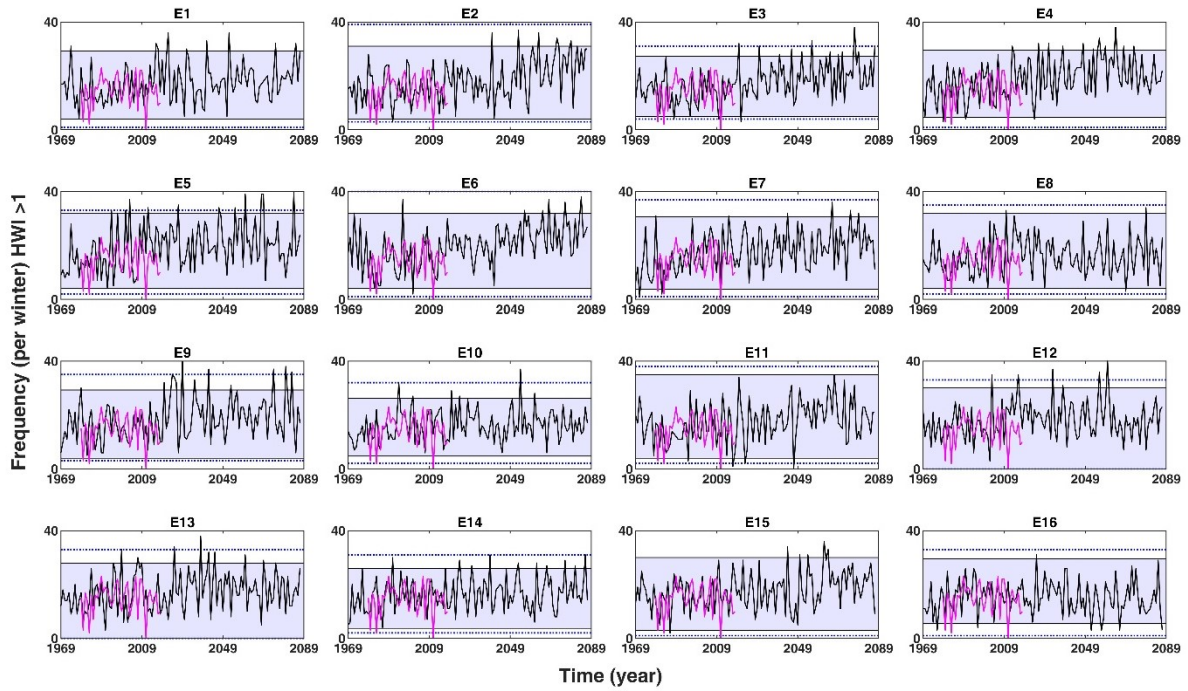
548 and anthropogenic climate change on the mean frequencies (see previous section) and trends
549 in frequencies (see next section) across different periods.

550 **6. Influence of the anthropogenic climate change and parametric effect on trends**

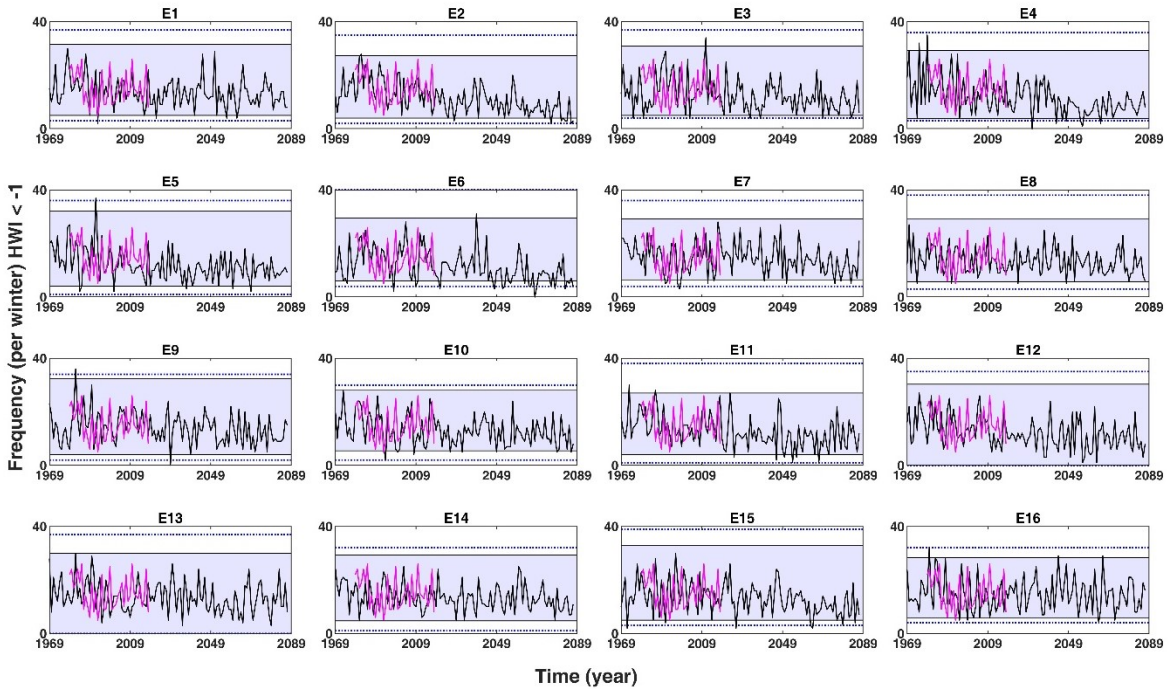
551 We discern the influence of the anthropogenic climate change and parametric effect on
552 the future projections of the trends in the frequency of haze conducive weather ($HWI > 1$) and
553 clear weather ($HWI < -1$). The time series of the haze conducive and clear weather frequency
554 from ERA-5 and the 16 PPE members for the historical and future periods is shown in Fig. 11
555 (a) and 11 (b). The 95th percentile values (blue shaded region) and the range (blue dotted lines)
556 in the haze conducive and clear weather frequency from the respective control simulation for
557 each PPE member are also shown.

558 For haze conducive weather ($HWI > 1$), the time series for selected PPE members (e.g.
559 E3, E4) show increasing positive trends. In particular, towards the end of the 21st century (Fig.
560 10a), the lower half of the control range is seldom sampled and more than the expected number
561 of values lie above the 97.5th percentile of the control frequencies. In contrast, for other PPE
562 members (e.g. E8, E10), the full time series sample the control distribution evenly throughout
563 the full period. For clear weather ($HWI < -1$), some members (e.g. E3, E4) show a clear
564 reduction during the 21st century whilst others (e.g. E16) show no trend and explore the control
565 distribution evenly (Fig 10b).

566 In Section 4, we examined the influence of anthropogenic climate change and
567 parametric effect on the mean frequencies. The analysis of mean frequencies provides an
568 estimate of the accumulated influence of climate change on frequencies with respect to the
569 control simulations whereas analysis of trends would provide a better estimate of changes
570 within a selected time period. Therefore, we apply the same analysis on the trends in the
571 frequencies (Fig. 11).



572



573

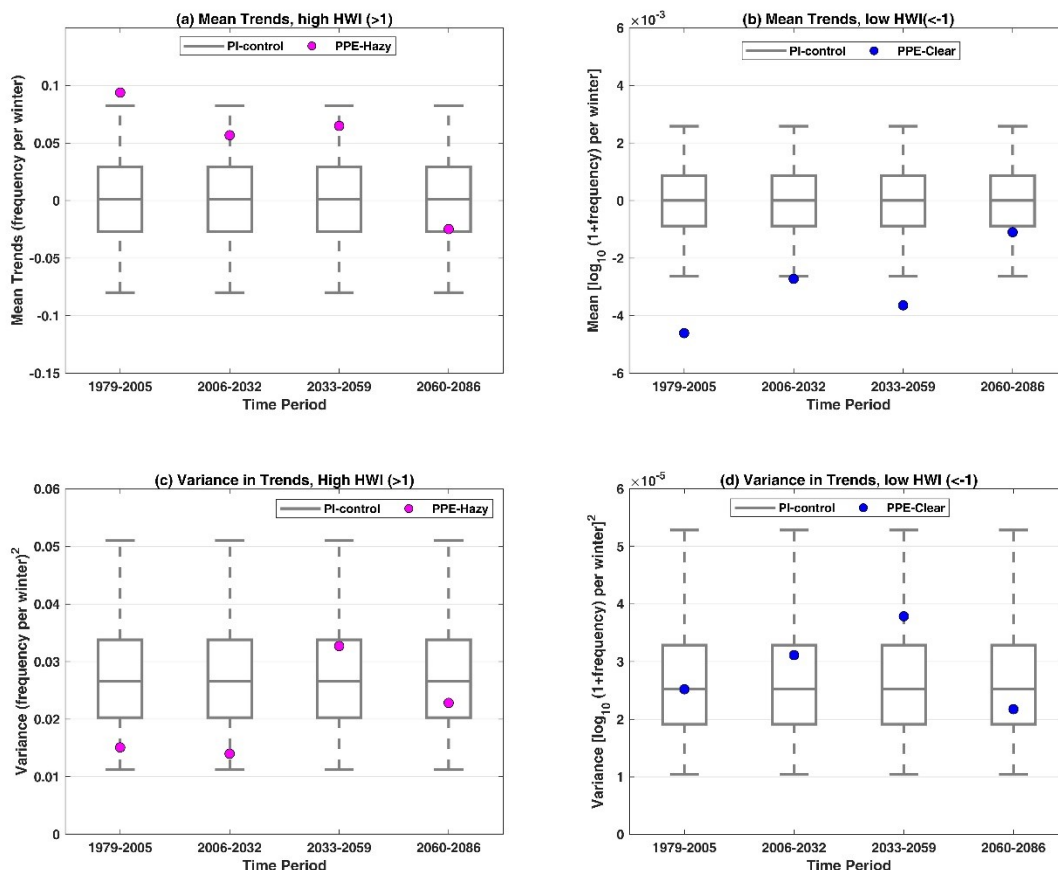
574 **Figure 10** Frequency of (a) haze conducive weather ($HWI > 1$) and (b) clear weather ($HWI < -1$) per
 575 per winter for individual PPE members (black line) under the historical and RCP8.5 scenarios for 1969-
 576 2087 and ERA5 reanalysis (pink line) for 1979-2018. Blue shaded region shows the 95th confidence
 577 interval and blue dashed line shows the range of the frequency of haze conducive and clear weather for
 578 the pre-industrial control simulation of 170-years.

579 We calculate the ensemble mean trend obtained from the 16 individual PPE member
580 trends to determine the influence of climate change for the historical period (see captions of
581 Fig. 11 for details). We describe the evolution of the historical trend for three equal-length
582 future time periods (i.e. near, mid and far future) and examine if the historical trends are
583 sustained across the 21st century and if the trends are discernible outside the range described
584 by the internal variability (Fig. 11a-b). The grey whiskers in Fig. 11 (a) and (b) cover the range
585 of trends that can be explained by internal variability and any trend values lying outside the
586 grey whiskers represent the influence of anthropogenic climate change.

587 The mean trend in the frequency of both haze conducive (HWI>1) and clear weather
588 (HWI <-1) for the historical period (1979-2005) lie outside the 95% confidence interval of the
589 control simulations. This suggests that the trends noted for the historical period cannot be
590 explained by internal variability alone and there is a substantial impact of anthropogenic
591 climate change on the historical trends. The trends in haze conducive weather lie within the
592 envelope of internal variability for the three future periods analysed here implying that the
593 historical trend is not sustained over the 21st century and indistinguishable from the internal
594 variability for the future. Figure 11 (a) also shows a positive mean trend in haze conducive
595 weather (HWI>1) for historical, near and mid future, but a weak negative trend for far future.
596 While the frequency of haze conducive weather increases for all three future periods with
597 respect to the historical period as shown in Fig. 6a, the trends only show an increment or
598 reduction for that period as these are not referenced to the historical period. Therefore, trends
599 could still be negative within any selected period, as in the case of the far future. In contrast,
600 the mean trends in clear weather frequency for near (2006-2032) and mid future (2033-2059)
601 lie outside the 95% confidence interval of the control simulation. This shows that for clear
602 weather frequency (HWI<-1), the historical trend is sustained over the first half of the 21st
603 century and then it levels off.

604 We now examine the influence of the parametric effect on the trends in the frequency
605 of haze conducive and clear weather. In Fig. 11 (c) and (d), we show the variance in trends for
606 the time series resampled using the control simulation (see captions for details on resampling).
607 The grey box and whiskers show the 95th confidence interval of the control variance used to
608 represent the internal variability. The variance in PPE trends calculated using 16 PPE members
609 for selected time periods is overlaid (circles). In Fig. 11 (c-d), if the variance for historical or
610 future periods lies outside the whiskers, we conclude an impact of the parametric effect on the
611 trends. However, if the variance across the 16 PPE members lies within the whiskers, we
612 conclude no impact of the parametric effect on the trend. Note that the variance in trends for
613 clear weather is in log-transformed space. As can be seen in Fig. 11c and 11d, the variance in
614 PPE trends for historical and future periods lies within the 95th percentile distribution of the
615 internal variability for both haze conducive and clear weather. Therefore, we do not find any
616 discernible influence of the parametric effect on the trends in the frequencies.

618



619
620

621

622 **Figure 11** Mean PPE trends for the frequency of **(a)** haze conducive weather ($\text{HWI}>1$) and **(b)**
623 clear weather ($\text{HWI}<-1$) for winter. Circles show the mean trends from 16 PPE members for
624 the historical (1979-2005) and near (2006-2032), mid (2033-2059) and far (2060-2086) future
625 under the RCP8.5 scenario. Grey box and whiskers show the distribution of 10,000 values of
626 trends sub-sampled from the control simulation. **(c-d)** same as (a-b) but mean is replaced by
627 variance in trends. For box and whiskers, we first randomly sampled 10,000 time series of
628 length 27 years using 2704 years of pre-industrial control simulation and calculated 10,000
629 values of trends. We then randomly sub-sample 16 trends values from the 10,000 trend values
630 and calculate the variance and mean of 16 trend values. The boxes are at the 25th and 75th
631 percentile and the whiskers at 2.5th and 97.5th percentile of mean and variance distribution. For
632 clear days, the frequencies were transformed to log space by applying a power transformation
633 of $\log_{10}(1+\text{frequency})$ before calculating trends.

634 7. Conclusions

635 In this study, we elucidate for the first time the influence of model physical
636 parametrisations, in addition to internal variability and climate change, on the future haze
637 conducive and clear weather conditions over the North China Plain (NCP) using the Perturbed
638 Parameter Ensemble (PPE) from the Met Office HadGEM3-GC3.05 model. We examine the
639 changes in winter (December-February) haze conducive and clear weather conditions for past
640 and future over the NCP using a large-scale meteorology-based daily Haze Weather Index
641 (HWI). We first identify the regional extent of the application of the HWI over China. We find
642 that the $\text{HWI}>1$ can be used as an indicator of haze conducive weather conditions and $\text{HWI}<-$
643 1 as an indicator of clear weather conditions for the entire NCP due to the spatial coherence of
644 regional meteorological conditions over this region.

645 The PPE shows that under the RCP8.5 emission scenario, the mean frequency of haze
646 conducive weather ($\text{HWI}>1$) can increase by up to ~65% in the near (2006-2032) and mid
647 (2033-2059) future and by ~87% in far future (2060-2086) as compared to the historical period
648 (1979-2005). In contrast, the frequency of clear weather ($\text{HWI}<-1$) can reduce by up to ~40%
649 in the near and mid-future and by ~57% in the far future. However, the opposite change of
650 relatively lower magnitude or negligible change in frequency of haze conducive and clear
651 weather, though less likely, is possible. The absolute number of days with haze conducive

652 weather in the far future can remain the same or up to ~ 3.5 times higher than the clear weather
653 over the NCP. There also exist a large interannual variability in the frequency of haze
654 conducive and clear weather conditions. However, no systematic change in the interannual
655 variance of the frequencies is noted in future as compared to the historical period. We also find
656 that the changes in the haze conducive weather ($\text{HWI} > 1$) for the future is associated with the
657 changes in the mid-tropospheric zonal wind component and strong vertical temperature
658 gradient between the lower to upper troposphere over the NCP. We find a consistently growing
659 influence of anthropogenic climate change and parametric effect on the mean haze conducive
660 and clear weather frequencies across the 21st century. This suggests that in addition to the
661 internal variability, the parametric effect adds as an additional source of uncertainty in future
662 projections of haze conducive and clear weather, particularly towards the end of the 21st
663 century. We find that the impact of anthropogenic climate change is discernible in trends for
664 the historical period for haze conducive weather and up to mid of the 21st century for clear
665 weather. Beyond these periods, the historical trends are not sustained and not distinguishable
666 from the internal variability.

667 This study considers four atmospheric variables to examine the changes in future haze
668 conducive and clear weather conditions, however, other atmospheric variables (e.g., boundary
669 layer height) or processes may influence the occurrence of haze. Furthermore, even though our
670 study shows the potential for an increase in haze conducive weather conditions and a reduction
671 in clear weather conditions for the future periods, the actual formation of haze will depend on
672 future emissions of air pollutants and their precursors. If the source emissions are cut-off or
673 reduced in the future, the risk of haze formation would naturally reduce. Nevertheless, the
674 projections of changes in the frequency and interannual variance in haze conducive weather
675 conditions can be very useful for developing successful adaptation and mitigation policies for
676 the future that consider both emissions and climate change, and therefore can be beneficial for

677 near and long-term planning and decision-making in relation to improving future PM_{2.5} air
678 quality.

679 **Data Availability**

680 The Copernicus Climate Change Service (C3S) (2017): ERA5: Fifth generation of ECMWF
681 atmospheric reanalyses of the global climate data are available through Copernicus Climate
682 Change Service Climate Data Store (CDS) (<https://cds.climate.copernicus.eu/>). The PM_{2.5}
683 concentrations for the US Embassy station in Beijing are archived at the following website
684 (<http://www.stateair.net/web/historical/1/1.html>). The haze weather index time series for PPE
685 and visibility data used in this paper can be obtained from the authors. The CAQRA dataset
686 can be freely downloaded at <https://doi.org/10.11922/sciencedb.00053>.

687 **Author Contribution**

688 SJ and RMD conceived and designed the manuscript; DS conducted PPE simulations using
689 Met Office HadGEM model; LP provided the visibility data; SJ performed data analysis,
690 produced figures, wrote the first draft; all co-authors provided comments on the manuscript
691 and contributed to writing.

692 **Competing interests**

693 The authors declare no financial or non-financial conflict of interest.

694 **Acknowledgements**

695 We thank Dr Li Ke for the discussion on the HWI calculation and Dr Peiqun Zhang for the
696 discussion on severe haze episodes in China. This work and its contributors (SJ, RMD, DS,
697 ST, ZS) were supported by the UK-China Research & Innovation Partnership Fund through
698 the Met Office Climate Science for Service Partnership (CSSP) China as part of
699 the Newton Fund (Met Office Reference Number: DN37368). RD and ZS also acknowledge

700 NERC for funding under the Atmospheric Pollution and Human Health Programme: Grant
701 Nos. NE/N006941/1 and NE/N007190/1. CL was supported by the National Key Research and
702 Development Program of China (Grant No. 2018YFA0606501). We also thank the two
703 reviewers for their constructive comments and suggestions on this manuscript.

704 **References**

705 An, Z., Huang, R. J., Zhang, R., Tie, X., Li, G., Cao, J., Zhou, W., Shi, Z., Han, Y., Gu, Z., and
706 Ji, Y.: Severe haze in northern China: A synergy of anthropogenic emissions and
707 atmospheric processes, *Proc Natl Acad Sci U S A*, 116, 8657-8666,
708 10.1073/pnas.1900125116, 2019.

709 Bai, N., Khazaei, M., van Eeden, S. F., and Laher, I.: The pharmacology of particulate matter
710 air pollution-induced cardiovascular dysfunction, *Pharmacology & therapeutics*, 113, 16-
711 29, 2007.

712 Cai, W., Li, K., Liao, H., Wang, H., and Wu, L.: Weather conditions conducive to Beijing
713 severe haze more frequent under climate change, *Nature Climate Change*, 7, 257-262,
714 10.1038/nclimate3249, 2017.

715 Callahan, C. W., Schnell, J. L., and Horton, D. E.: Multi-index attribution of extreme winter
716 air quality in Beijing, China, *Journal of Geophysical Research: Atmospheres*, 124, 4567-
717 4583, 2019.

718 Callahan, C. W., and Mankin, J. S.: The Influence of Internal Climate Variability on Projections
719 of Synoptically Driven Beijing Haze, *Geophysical Research Letters*, 47,
720 10.1029/2020gl088548, 2020.

721 Chen, H., and Wang, H.: Haze days in North China and the associated atmospheric circulations
722 based on daily visibility data from 1960 to 2012, *Journal of Geophysical Research:*
723 *Atmospheres*, 120, 5895-5909, 2015.

724 Deser, C., Knutti, R., Solomon, S., and Phillips, A. S.: Communication of the role of natural
725 variability in future North American climate, *Nature Climate Change*, 2, 775-779, 2012.

726 Deser, C., Phillips, A. S., Alexander, M. A., and Smoliak, B. V.: Projecting North American
727 climate over the next 50 years: Uncertainty due to internal variability, *Journal of Climate*,
728 27, 2271-2296, 2014.

729 Han, Z., Zhou, B., Xu, Y., Wu, J., and Shi, Y.: Projected changes in haze pollution potential in
730 China: an ensemble of regional climate model simulations, *Atmospheric Chemistry and
731 Physics*, 17, 10109-10123, 10.5194/acp-17-10109-2017, 2017.

732 Hawkins, E., and Sutton, R.: Time of emergence of climate signals, *Geophysical Research
733 Letters*, 39, n/a-n/a, 10.1029/2011gl050087, 2012.

734 He, J., Yu, Y., Xie, Y., Mao, H., Wu, L., Liu, N., and Zhao, S.: Numerical model-based
735 artificial neural network model and its application for quantifying impact factors of urban
736 air quality, *Water, Air, & Soil Pollution*, 227, 1-16, 2016.

737 Hersbach, H., Bell, B., Berrisford, P., Hirahara, S., Horányi, A., Muñoz-Sabater, J., Nicolas,
738 J., Peubey, C., Radu, R., Schepers, D., Simmons, A., Soci, C., Abdalla, S., Abellan, X.,
739 Balsamo, G., Bechtold, P., Biavati, G., Bidlot, J., Bonavita, M., Chiara, G., Dahlgren, P.,
740 Dee, D., Diamantakis, M., Dragani, R., Flemming, J., Forbes, R., Fuentes, M., Geer, A.,
741 Haimberger, L., Healy, S., Hogan, R. J., Hólm, E., Janisková, M., Keeley, S., Laloyaux,
742 P., Lopez, P., Lupu, C., Radnoti, G., Rosnay, P., Rozum, I., Vamborg, F., Villaume, S.,
743 and Thépaut, J. N.: The ERA5 global reanalysis, *Quarterly Journal of the Royal
744 Meteorological Society*, 146, 1999-2049, 10.1002/qj.3803, 2020.

745 Hong, C., Zhang, Q., Zhang, Y., Davis, S. J., Tong, D., Zheng, Y., Liu, Z., Guan, D., He, K.,
746 and Schellnhuber, H. J.: Impacts of climate change on future air quality and human health
747 in China, *Proceedings of the National Academy of Sciences*, 116, 17193-17200, 2019.

748 Hou, P., and Wu, S.: Long-term changes in extreme air pollution meteorology and the
749 implications for air quality, *Scientific reports*, 6, 1-9, 2016.

750 Jia, B., Wang, Y., Yao, Y., and Xie, Y.: A new indicator on the impact of large-scale circulation
751 on wintertime particulate matter pollution over China, *Atmospheric Chemistry and*
752 *Physics*, 15, 11919-11929, 2015.

753 Kan, H., London, S. J., Chen, G., Zhang, Y., Song, G., Zhao, N., Jiang, L., and Chen, B.:
754 Differentiating the effects of fine and coarse particles on daily mortality in Shanghai,
755 China, *Environment international*, 33, 376-384, 2007.

756 Kan, H., Chen, R., and Tong, S.: Ambient air pollution, climate change, and population health
757 in China, *Environment international*, 42, 10-19, 2012.

758 Kay, J. E., Deser, C., Phillips, A., Mai, A., Hannay, C., Strand, G., Arblaster, J. M., Bates, S.,
759 Danabasoglu, G., and Edwards, J.: The Community Earth System Model (CESM) large
760 ensemble project: A community resource for studying climate change in the presence of
761 internal climate variability, *Bulletin of the American Meteorological Society*, 96, 1333-
762 1349, 2015.

763 Knutti, R., Furrer, R., Tebaldi, C., Cermak, J., and Meehl, G. A.: Challenges in combining
764 projections from multiple climate models, *Journal of Climate*, 23, 2739-2758, 2010.

765 Kong, L., Tang, X., Zhu, J., Wang, Z., Li, J., Wu, H., Wu, Q., Chen, H., Zhu, L., and Wang,
766 W.: A 6-year-long (2013–2018) high-resolution air quality reanalysis dataset in China
767 based on the assimilation of surface observations from CNEMC, *Earth System Science*
768 *Data*, 13, 529-570, 2021.

769 Li, K., Liao, H., Cai, W., and Yang, Y.: Attribution of Anthropogenic Influence on
770 Atmospheric Patterns Conducive to Recent Most Severe Haze Over Eastern China,
771 *Geophysical Research Letters*, 45, 2072-2081, 10.1002/2017gl076570, 2018.

772 Li, Q., Zhang, R., and Wang, Y.: Interannual variation of the wintertime fog–haze days across
773 central and eastern China and its relation with East Asian winter monsoon, *International*
774 *Journal of Climatology*, 36, 346-354, 2016.

775 Liu, C., Zhang, F., Miao, L., Lei, Y., and Yang, Q.: Future haze events in Beijing, China: When
776 climate warms by 1.5 and 2.0°C, *International Journal of Climatology*, 40, 3689-3700,
777 10.1002/joc.6421, 2019.

778 Liu, Q., Jia, X., Quan, J., Li, J., Li, X., Wu, Y., Chen, D., Wang, Z., and Liu, Y.: New positive
779 feedback mechanism between boundary layer meteorology and secondary aerosol
780 formation during severe haze events, *Scientific reports*, 8, 1-8, 2018.

781 Liu, T., Gong, S., He, J., Yu, M., Wang, Q., Li, H., Liu, W., Zhang, J., Li, L., Wang, X., Li, S.,
782 Lu, Y., Du, H., Wang, Y., Zhou, C., Liu, H., and Zhao, Q.: Attributions of meteorological
783 and emission factors to the 2015 winter severe haze pollution episodes in China's Jing-
784 Jin-Ji area, *Atmospheric Chemistry and Physics*, 17, 2971-2980, 10.5194/acp-17-2971-
785 2017, 2017.

786 Pei, L., Yan, Z., Sun, Z., Miao, S., and Yao, Y.: Increasing persistent haze in Beijing: potential
787 impacts of weakening East Asian winter monsoons associated with northwestern Pacific
788 sea surface temperature trends, *Atmospheric Chemistry and Physics*, 18, 3173-3183,
789 2018.

790 Pendergrass, D., Shen, L., Jacob, D., and Mickley, L.: Predicting the impact of climate change
791 on severe wintertime particulate pollution events in Beijing using extreme value theory,
792 *Geophysical Research Letters*, 46, 1824-1830, 2019.

793 Petäjä, T., Järvi, L., Kerminen, V.-M., Ding, A., Sun, J., Nie, W., Kujansuu, J., Virkkula, A.,
794 Yang, X., and Fu, C.: Enhanced air pollution via aerosol-boundary layer feedback in
795 China, *Scientific reports*, 6, 1-6, 2016.

796 Qiu, L., Yue, X., Hua, W., and Lei, Y.-D.: Projection of weather potential for winter haze
797 episodes in Beijing by 1.5 °C and 2.0 °C global warming, *Advances in Climate Change*
798 *Research*, 11, 218-226, 10.1016/j.accre.2020.09.002, 2020.

799 Renhe, Z., Li, Q., and Zhang, R.: Meteorological conditions for the persistent severe fog and
800 haze event over eastern China in January 2013, *Science China Earth Sciences*, 57, 26-35,
801 2014.

802 Sexton, D. M., McSweeney, C. F., Rostron, J. W., Yamazaki, K., Booth, B. B., Murphy, J. M.,
803 Regayre, L., Johnson, J. S., and Karmalkar, A. V.: A perturbed parameter ensemble of
804 HadGEM3-GC3. 05 coupled model projections: part 1: selecting the parameter
805 combinations, *Climate Dynamics*, 56, 3395-3436, 2021.

806 Shen, L., Jacob, D. J., Mickley, L. J., Wang, Y., and Zhang, Q.: Insignificant effect of climate
807 change on winter haze pollution in Beijing, *Atmospheric Chemistry and Physics*, 18,
808 17489-17496, 10.5194/acp-18-17489-2018, 2018.

809 Sun, Y., Jiang, Q., Wang, Z., Fu, P., Li, J., Yang, T., and Yin, Y.: Investigation of the sources
810 and evolution processes of severe haze pollution in Beijing in January 2013, *Journal of*
811 *Geophysical Research: Atmospheres*, 119, 4380-4398, 2014.

812 Tie, X., Huang, R.-J., Cao, J., Zhang, Q., Cheng, Y., Su, H., Chang, D., Pöschl, U., Hoffmann,
813 T., and Dusek, U.: Severe pollution in China amplified by atmospheric moisture,
814 *Scientific Reports*, 7, 1-8, 2017.

815 Wang, J.-L., Zhang, Y.-h., Shao, M., Liu, X.-l., Zeng, L.-m., Cheng, C.-l., and Xu, X.-f.:
816 Quantitative relationship between visibility and mass concentration of PM_{2.5} in Beijing,
817 *Journal of environmental sciences*, 18, 475-481, 2006.

818 Wang, L., Wei, Z., Yang, J., Zhang, Y., Zhang, F., Su, J., Meng, C., and Zhang, Q.: The 2013
819 severe haze over southern Hebei, China: model evaluation, source apportionment, and
820 policy implications, *Atmospheric Chemistry and Physics*, 14, 3151-3173, 2014a.

821 Wang, Y., Yao, L., Wang, L., Liu, Z., Ji, D., Tang, G., Zhang, J., Sun, Y., Hu, B., and Xin, J.:
822 Mechanism for the formation of the January 2013 heavy haze pollution episode over
823 central and eastern China, *Science China Earth Sciences*, 57, 14-25, 2014b.

824 Xu, M., Chang, C. P., Fu, C., Qi, Y., Robock, A., Robinson, D., and Zhang, H. m.: Steady
825 decline of east Asian monsoon winds, 1969–2000: Evidence from direct ground
826 measurements of wind speed, *Journal of Geophysical Research: Atmospheres*, 111, 2006.

827 Xu, P., Chen, Y., and Ye, X.: Haze, air pollution, and health in China, *Lancet*, 382, 2067,
828 10.1016/S0140-6736(13)62693-8, 2013.

829 Yamazaki, K., Sexton, D. M., Rostron, J. W., McSweeney, C. F., Murphy, J. M., and Harris,
830 G. R.: A perturbed parameter ensemble of HadGEM3-GC3. 05 coupled model
831 projections: part 2: global performance and future changes, *Climate Dynamics*, 56, 3437-
832 3471, 2021.

833 Yin, Z., and Wang, H.: Role of atmospheric circulations in haze pollution in December 2016,
834 *Atmospheric Chemistry and Physics*, 17, 11673-11681, 10.5194/acp-17-11673-2017,
835 2017.

836 Zhang, Q., Ma, Q., Zhao, B., Liu, X., Wang, Y., Jia, B., and Zhang, X.: Winter haze over North
837 China Plain from 2009 to 2016: Influence of emission and meteorology, *Environ Pollut*,
838 242, 1308-1318, 10.1016/j.envpol.2018.08.019, 2018.

839 Zhang, R., Jing, J., Tao, J., Hsu, S.-C., Wang, G., Cao, J., Lee, C. S. L., Zhu, L., Chen, Z., and
840 Zhao, Y.: Chemical characterization and source apportionment of PM 2.5 in Beijing:
841 seasonal perspective, *Atmospheric Chemistry and Physics*, 13, 7053-7074, 2013.

842 Zhang, L., Wilcox, L. J., Dunstone, N. J., Paynter, D. J., Hu, S., Bollasina, M., ... & Zou, L.
843 (2021). Future changes in Beijing haze events under different anthropogenic aerosol
844 emission scenarios. *Atmospheric Chemistry and Physics*, 21(10), 7499-7514.

845 Zhang, Z., Gong, D., Mao, R., Kim, S. J., Xu, J., Zhao, X., and Ma, Z.: Cause and predictability
846 for the severe haze pollution in downtown Beijing in November-December 2015, *Sci*
847 *Total Environ*, 592, 627-638, 10.1016/j.scitotenv.2017.03.009, 2017.

848

849